




Production of hydrogen gas sensors based on sol–gel spin-coated Nb₂O₅ thin films

H. Akkaya Komurcu^{1,2,*} , T. Ataser^{1,3}, N. Akin Sonmez^{1,3}, T. Asar^{1,4}, and S. Ozcelik^{1,3}

¹ Photonics Application and Research Center, Gazi University, 06500 Ankara, Turkey

² Department of Photonics Science and Engineering, Graduate School of Natural and Applied Science, Gazi University, 06500 Ankara, Turkey

³ Department of Photonics, Faculty of Applied Sciences, Gazi University, 06500 Ankara, Turkey

⁴ Department of Physics, Faculty of Science, Gazi University, 06500 Ankara, Turkey

Received: 29 November 2022

Accepted: 25 March 2023

Published online:
10 April 2023

© The Author(s), under exclusive licence to Springer Science+Business Media, LLC, part of Springer Nature 2023

ABSTRACT

In the present work, single-layer and multi-layer Nb₂O₅ thin films were obtained by using sol–gel spin-coating technique and applying annealing temperature. The formation of hydroxyl on the Nb₂O₅ surface was determined by the FTIR technique. It is seen the structure turns into pure Nb₂O₅ form above 350 °C. Thickness effects on the structural and morphological properties of the annealed films were investigated by SIMS, XRD, XPS and AFM measurements. The thicknesses of the 1, 2 and 3-layered films are 65, 108 and 178 nm, respectively, and Nb₂O₅ films have amorphous structures even at an annealing temperature of 350 °C. RMS surface roughness of the films increased with increasing the film thickness increasing the stacked layers, while the 2-layered film has the highest surface area. After the characterizations have been defined, Ag interdigital electrodes were fabricated on the developed films with the Aerosol Jet Printing technique to produce H₂ gas sensors whose active material is single-layer and multi-layer Nb₂O₅ thin films. The sensing performances of the sensors were examined with respect to film thickness under H₂ concentrations ranging from 90 to 1200 ppm at operating temperature of 25 °C. Based on the 2-layered film, the sensor shows better hydrogen sensitivity, which can be at least partially caused by the higher surface area of the films and also associate with thickness of 108 nm. In addition, all fabricated sensors have good selectivity to H₂ gas compared to the other gases such as CO, O₂ and C₃H₈, as well as long-term stability over 90 days.

Address correspondence to E-mail: akkayahuda@gmail.com

1 Introduction

Transition metal oxide materials are an important class of semiconductor materials because of their technological application fields such as catalysts, light-emitting diodes, solar cells, optical smart windows, batteries, electrochromic devices, memristive and gas sensors [1–3]. Niobium oxide, one of the transition metal oxides is a strategic high-technology group V–B oxide material [4]. It is mainly found in the combination of niobium with oxygen as stoichiometric oxides such as NbO, NbO₂, and Nb₂O₅, the last one is the thermodynamically stable form with the lowest free energy of formation. Nb₂O₅ has different crystal structures: Nb₂O₅·n-H₂O (amorphous), TT-Nb₂O₅ (pseudo-hexagonal), T-Nb₂O₅ (orthorhombic), and H-Nb₂O₅ (monoclinic) [5]. The different phases are formed depending on the production method of the compound, temperature, and oxygen spaces. While the amorphous phase is generally observed at temperatures below 500 °C, the orthorhombic phase is formed at temperatures between 500 and 900 °C and the crystal structure determined for heat treatments above 1000 °C is the monoclinic phase which is the most thermodynamically stable [6]. Nb₂O₅ is an n-type direct semiconductor with a wide band gap (3.4 eV), so appropriate to use as a photocatalyst under UV light. They can also use it as cathodic electrochromic material with stability and reversibility and it changes its color when reduced. Besides, either optical or electrical gas sensors can develop using Nb₂O₅ electrochromic materials. Electrical conductivity of the Nb₂O₅-based electrical gas sensors changes when exposed to gases such as oxygen (O₂), dissolved O₂, carbon monoxide (CO), ammonia (NH₃), hydrogen (H₂) and several hydrocarbons (HCs) gases.

A lot of researchers have focused on the thin film form of Nb₂O₅ because of its excellent physical, optical, and chemical properties, such as high refractive index, low extinction coefficient, excellent thermodynamic and chemical stability, and high transparency in the UV–vis–NIR region of the electromagnetic spectrum [7]. Nb₂O₅ thin films can be prepared by a variety of methods such as electron beam evaporation [8], chemical spray pyrolysis [9], atomic layer deposition [10], sputtering techniques [11], and sol–gel method [12]. From these processes, the sol–gel coating has attracted great attention due to its low crystallization temperature and

homogeneity at the molecular level. It is also a very useful method for obtaining both inorganic and organic polymers. This system has some advantages, such as control of chemical composition, high homogeneity, ease of formation of multi-layer coatings, and energy-saving [13]. Even more remarkable is that the sol–gel spin-coating technique is also beneficial in lowering the production cost of multi-layer Nb₂O₅ thin films. The properties of the sol–gel spin-coated multi-layer Nb₂O₅ thin films can be easily and quickly investigated by changing the number, thickness chemical composition, etc., for each layer.

Based on the literature survey, there are many both single-layer and multi-layer thin film coatings works achieved with sol–gel coating technique, which is an economical and fast coating technique, up to now. Increasing the thickness of these films can be achieved by controlling some sol–gel parameters or by dropping the sol–gel solution droplets on the substrate according to the number of layers. For example, by changing the number of TiO₂ and ZnO spinning cycles some observed that the materials have shown electrical, optical, and structural changes [14, 15]. When the number of TiO₂ layers increased, a decrease was determined in its electrical resistance, or with increasing the number of ZnO layers, the optical band gap energy decreased. However, to the best of our knowledge, there is no study involving the coating of Nb₂O₅ material on the substrate with a sol–gel spin-coating system by increasing the number of layers, i.e. increasing the cycles. This is the first work which is to examine of influence the number of layers on the characteristics of the Nb₂O₅ films, as well as present comparisons among the stacked layers. In addition, it is worth remarking that the material properties of the Nb₂O₅ films can be controlled with film thickness which in turn will affect the gas sensor properties because sensing performances of the sensors are strongly influenced by the morphology, porosity and large surface-to-volume ratio of the films.

Up to now, Nb₂O₅ thin films have not been sufficiently studied in the field of gas sensors, so very little information is available in the literature about them. Hyodo et al. [16] fabricated the H₂ gas sensors based on anodically oxidized Nb₂O₅ film coupling with noble metal electrodes and reported the sensitivity of the sensors at 100 °C. Rani et al. [17] investigated the behaviors and sensing performances of

the H₂ sensors based on nanoporous Nb₂O₅ films at different concentrations, and temperatures from RT to 100 °C. So, it is clearly seen that the results of sensitive, stable and selective H₂ sensor production based on sol–gel spin-coated Nb₂O₅ thin films have been brought to the literature for the first time with our study.

Hence, first, it was discussed the results according to changes in the film thickness of sol–gel spin-coated Nb₂O₅ thin films, and then, coming to the curious part where it was reported the H₂ gas sensing properties of the single-layer and multi-layer films. In order to determine the selectivity, the obtained sensors were also investigated under carbon-monoxide (CO), oxygen (O₂) and propane (C₃H₈) gases. In addition, the stability performances of the sensors were also investigated.

2 Experimental details

2.1 Preparation and characterization of Nb₂O₅ thin films

The sol–gel spin coating technique was used to develop single-layer and multi-layer niobium pentoxide (Nb₂O₅) thin films on silicon (Si) substrates. To get the viscous solution, 1.6 g NbCl₅ was dissolved in 33.2 ml ethanol and 0.68 ml distilled water. The mixture was stirred at room temperature (RT) with the help of a magnetic stirrer for 24 h at 500 rpm to get a homogeneous, transparent, and stable solution. First, a drop of this solution was dropped onto Si substrates, and coated in a spin coating system having a speed of 3500 rotation/s for 30 s. After coating, obtained single-layer film was sintered to dry on the heater at 120 °C for 30 min. The above procedure was repeated 2 and 3 times to make thin films with multi-layer. The schematic illustration of the steps involved in the coated process of the films is given in Fig. 1. In addition, hydrated niobium pentoxide (Nb₂O₅•nH₂O) films may occur as a result of preparation in an aqueous environment. In order to avoid this, the prepared films were annealed at 200 and 350 °C, finally. Fourier transform infrared (FTIR, Bruker Vertex-80) absorbance spectroscopy was applied to identify the molecular structure of the films (both sintered and annealed). FTIR spectrum was obtained between 400 and 4000 cm⁻¹ with a resolution of 4 cm⁻¹ at room temperature. Secondary ion mass

spectrometry (SIMS, Hiden Analytical) depth profile analyses were carried out to determine the thickness, interfaces, and atomic distribution of the annealed films. During the SIMS experiments, the base pressure of the chamber was kept at 10⁻¹⁰ mbar.

The sputter parameter of O₂ ion gun was set to 5 keV energy, 400 nA beam current. SIMS crater thicknesses were measured with a stylus-type profilometer (Veeco, Dektak-150). X-ray diffraction (XRD, APD 2000 PRO XRD) measurements were performed using CuKα1 X-ray source ($\lambda = 1.54052 \text{ \AA}$) to identify the crystalline phase of the annealed films. X-ray Photoelectron Spectroscopy (XPS, Omicron) analysis was carried out with monochromatic MgKα (hν = 1253.6 eV) irradiation to characterize the chemical bonding structure of the annealed films. The main parameters of XPS were: 25 W beam power; 10 mm beam size; and 45° emission angle. The pass energy of the X-ray beam was 20 eV and the step size was 0.1 eV. The pressure in the analytical chamber during spectral acquisition was about 10⁻⁹ mbar. XPS data was calibrated against C 1s core level peak (binding energy, 285.0 eV). The surface morphology and the RMS surface roughness were estimated by a high-performance atomic force microscope (hp-AFM, Nano Magnetics Instruments) using dynamic scanning mode. The AFM scan area was 3 × 3 μm, and the scan speed was 2 μm s⁻¹. All analyses were carried out at room temperature.

2.2 Sensor fabrication and measurement set-up

The sensors are composed of two parts, namely: interdigital electrodes (IDE) and the active material (single-layer and multi-layer Nb₂O₅ thin films prepared at 200 and 350 °C). Both patterns of the IDE and active area of the H₂ gas sensor design were first drawn on AutoCAD and were fed to the 3D printer. Then, Optomec Aerosol Jet 5X System was used to print them on the surface of the Nb₂O₅ thin films a schematic diagram of the printing process is illustrated in Fig. 2, and one of the fabricated sensors is also presented inset in this figure. A commercially available silver (Ag) ink (novacentrix JS-A102A AP, 40% solid weight) was used for printing and it was aerosolized using an ultrasonic atomizer. The diameter of the aerosolized droplets is about 1–5 μm, while the diameter of the Nozzle is 200 μm. The

Fig. 1 Production steps of the Nb₂O₅ thin films

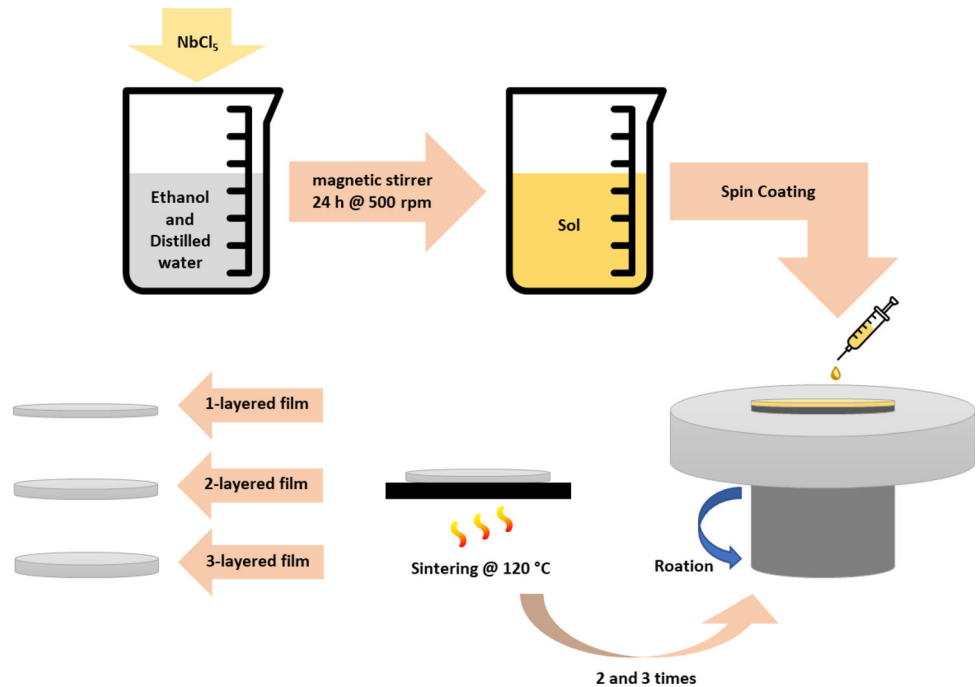
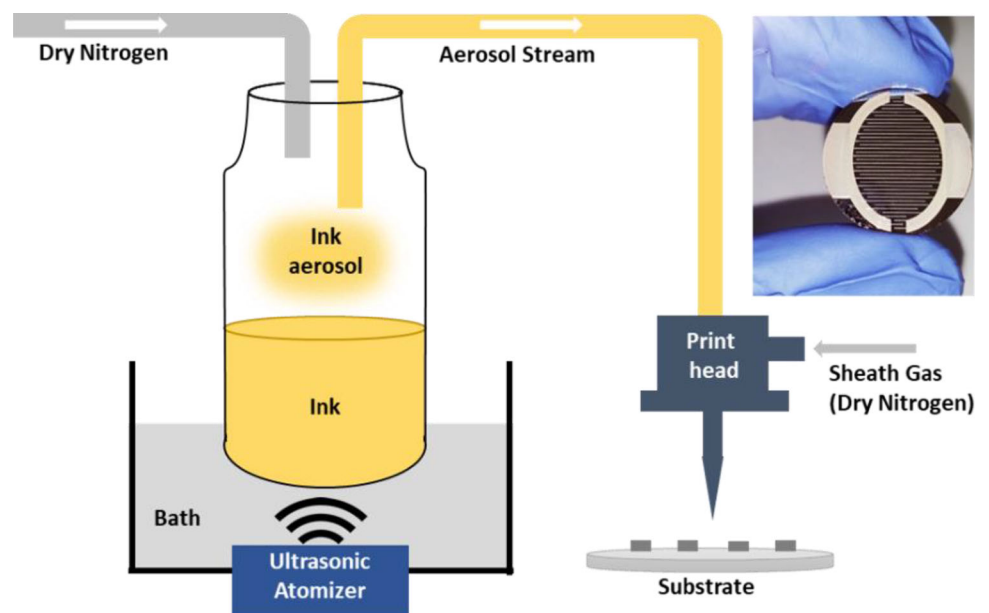


Fig. 2 A schematic diagram of the Aerosol Jet Printing (AJP) process with an ultrasonic atomizer, and a fabricated sensor image



droplets flowed to the print head where they were surrounded by secondary gas, known as the sheath gas, and directed towards the substrate with the nozzle. Then, they reached the Nb₂O₅ thin films passing through the nozzle. N₂ gas was used for both the carrier and sheath flows. The process parameters used during printed of Ag ink in this work are given in Table 1.

Table 1 Printing parameters of the AJP system

Parameter	Ag
Nozzle Diameter (μm)	200
Atomizer Flow Rate (sccm)	20
Sheath Gas Flow Rate (sccm)	57
Platen Temperature (°C)	60
Process Speed (mm/s)	10

After that, the printed Ag interdigital electrodes were sintered at 200 °C for 60 min to reach the required conductivity of the electrodes. The electrode lines are about 65 μm wide and about 7 μm thick. For convenience, sensors produced from the Nb_2O_5 thin films with 1, 2 and 3 layers at a temperature of 200 °C; were named Sensor1-200, Sensor2-200, and Sensor3-200, respectively. Likewise, sensors produced at 350 °C were named Sensor1-350, Sensor2-350, and Sensor3-350, respectively. The H_2 gas sensing properties of the developed sensors based on the Nb_2O_5 thin films were performed through a home-made gas sensor testing system. The sensors were sequentially placed onto a chamber in a 25 L. Meanwhile, the gas flow to the chamber was controlled by using mass flow controllers. The sensor electrodes were externally connected to a digital multimeter and the sensor signal was periodically monitored in terms of resistance in dry air and in H_2 gas by a Fluke View Forms Version 3.6.

3 Results and discussion

3.1 Structural and morphological properties of Nb_2O_5 thin films

FTIR spectroscopy is an ideal technique for identifying functional groups that may occur in any material. So, in order to evaluate the dehydration and determine the molecular structure of the sol-gel spin-coated Nb_2O_5 thin films both sintered at 120 °C and annealed at 200 and 350 °C, FTIR absorption spectra was carried out in the range of 400–4000 cm^{-1} , as shown in Fig. 3. In the IR region of the FTIR spectra,

the observed peaks in the bands at 600–950 cm^{-1} can be attributed to characteristic peaks for niobium-oxide bonds. The peak in this band located at around 621 cm^{-1} is attributed to the symmetric stretching of Nb–Nb–O bonds [18, 19]. The other peak band lies between 800 and 950 cm^{-1} and corresponds to stretches of the Nb–O [20]. However, only differently, the peak located at around 612 cm^{-1} corresponds Si–Si stretching [21]. The observed peak at around 1100 cm^{-1} can be attributed to the Si–O vibration mode due to the oxidation of the Si substrate [22, 23]. In addition, a broad absorption band centered at 3000 cm^{-1} was observed for Nb_2O_5 thin film sintered at 120 °C. This band is attributed to Nb–OH vibration and O–H stretching vibration of water molecules comes from the solution [20, 24]. This low intensity of absorption band shows that the dehydration of the structure starts at 120 °C. The above-mentioned hydroxyl band was extremely reduced annealed at 200 °C, and completely disappeared in the annealed at 350 °C. Thus, it can be said that the structure turns into pure Nb_2O_5 form [20, 25]. As a result of FTIR analysis, considering the application of 200 °C sintering temperature during the fabrication of the electrodes in the sensor part, structural and surface analysis experiments of the films, were carried out without considering the film sintered at 120 °C.

SIMS depth profile analyses with a detection limit in the order of 1 ppm were carried out to determination of the Nb_2O_5 thin film thickness, as well the film/substrate interfaces and the atomic distribution of that Nb element in the layer of the films. In SIMS analyses, the films were bombarded with an oxygen ion beam with 5 keV energy, so, the profiles of

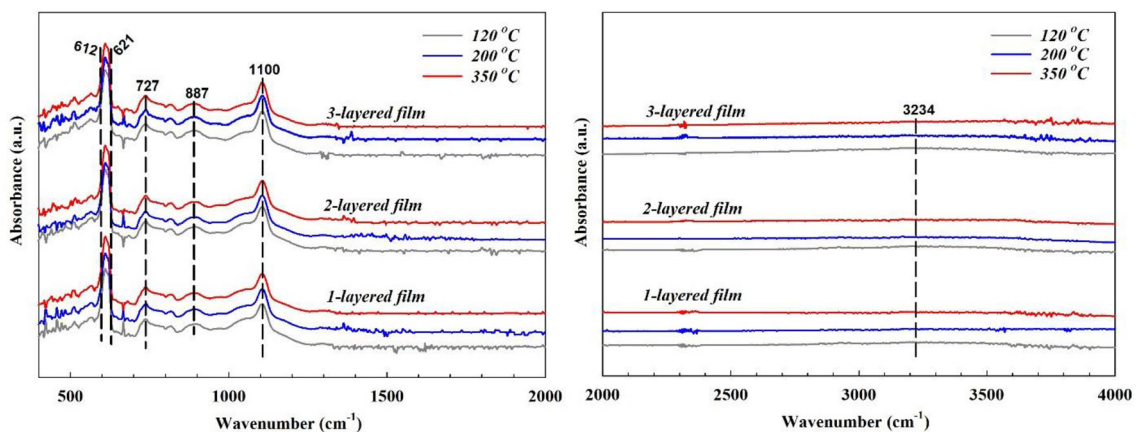


Fig. 3 FTIR spectra of both sintered and annealed Nb_2O_5 thin films

niobium (Nb) and silicon (Si) elements could be observed, but the oxygen (O) element could not be followed naturally during the experiment. Figure 4 shows SIMS depth profiles of the single-layer and multi-layer Nb_2O_5 thin films on Si substrates annealed at 200 and 350 °C. Nb distributions within the whole thickness of all films are very uniform and have good homogeneity and Nb/Si interface has a sharp border. In addition, the thicknesses of the 1, 2 and 3-layered films are 65, 108 and 178 nm, respectively. It is an expected result that the thickness of the films will increase by increasing the number of Nb_2O_5 spinning cycles.

Nb_2O_5 thin films were annealed at low temperatures in this work. So, it was expected to obtain an amorphous structure while avoiding cost-increasing or number-increasing processes. It is easily thought that the amorphous structure of the Nb_2O_5 films will have a positive effect on the sensitivity of a gas sensor to be developed based on these films. The amorphous structure is more disordered than that of crystal structure (no having big grains), so having a lot of

oxygen vacancies and defects or interstitial positions which provides many more local donor energy levels. These donor energy levels increase conductivity, thanks to the concentration of the charge carrier, so the sensitivity of the gas sensor increases according to the crystal structure. Zhang et al. [26] in their work, point out that gas sensing materials with amorphous structures are important in the development of sensors with high selectivity and excellent performance. Considering the importance of this, XRD analyses were performed for the confirmation of the crystal structure of the Nb_2O_5 thin films. Figure 5 shows XRD patterns of the single-layer and multi-layer Nb_2O_5 thin films on Si substrates annealed at 350 °C. As clear from the figure, obtained Nb_2O_5 films have amorphous structures. This is to be expected given the comparatively low temperature (below 500 °C) because the phase transformations of Nb_2O_5 strongly depend on the high temperature [27, 28]. It is known from the literature that it is necessary to apply an annealing temperature above 500 °C in order for Nb_2O_5 to show a certain crystal phase [25, 29]. That is, it is an expected result that there is no any Nb_2O_5

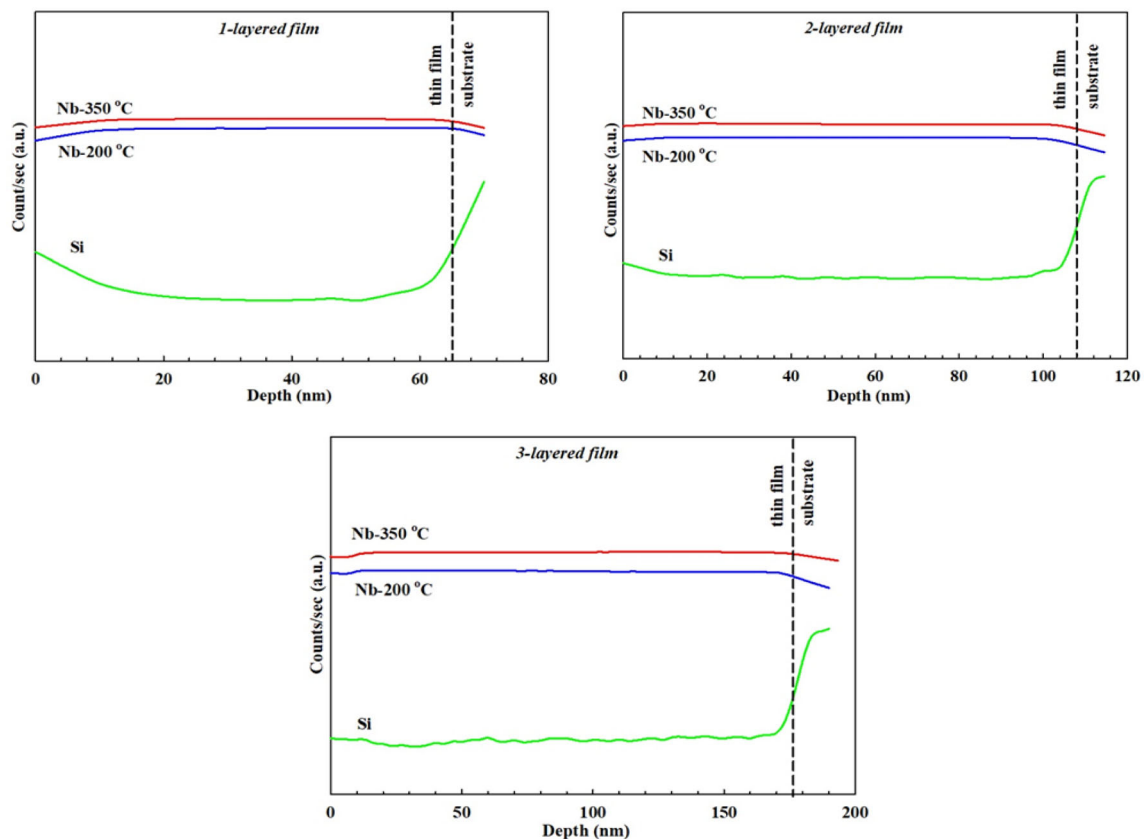


Fig. 4 SIMS depth profiles of annealed Nb_2O_5 thin films

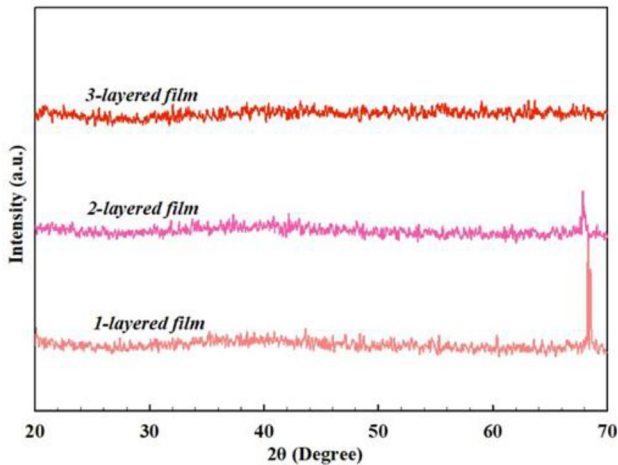


Fig. 5 XRD patterns of the single-layer and multi-layer Nb_2O_5 thin films annealed at 350 °C

phase peak on the Fig. 1 (TT- Nb_2O_5 (pseudo-hexagonal, JCPDS 07-0061), T- Nb_2O_5 (orthorhombic, JCPDS 27-1003), and H- Nb_2O_5 (monoclinic, JCPDS 72-1297). In addition, the peak observed at around $2\theta = 69^\circ$ are consistent with that of pure Si (400) phase (JCPDS 01-0787) which is attributed to the substrate.

XPS is a very powerful technique used to elucidate the elemental analysis and bonding nature of the constituent species on the top surface layers of the films. In this work, XPS analysis was performed in order to confirm the presence of the phase of Nb_2O_5 thin films coated on Si substrate. Figure 6 shows the XPS spectrum consisting of Nb 3d and O 1s core levels for Nb_2O_5 thin films prepared at different film thicknesses annealed at 200 and 350 °C. The binding

energy of around 206, 209 and 530 eV for $\text{Nb}^{5+}3d_{5/2}$, $\text{Nb}^{5+}3d_{3/2}$ and O1s, respectively, verify the phase formation of Nb_2O_5 [30, 31]. In addition, as reported in the literature [25], the Nb 3d major peak appears to shift to lower binding energy with increasing annealing temperature. Similarly, the O 1s binding energy decreased slightly with temperature. This can be attributed to the decrease in the amount of oxygen on the surface by the dehydration process at 350 °C [25].

The morphology, porosity and surface area of the Nb_2O_5 thin films are directly related to the gas sensitivity of the sensors to be developed based on these films. Because gas diffusion and transport are affected by the surface of the films. Gas detection of the sensor becomes easier and faster when there are more absorption sites for the target gas at the surface. For this reason, the surface properties of Nb_2O_5 thin films were investigated by AFM measurements and in the next part of the article, the relationship between the film surface and sensor sensitivity was also discussed. Figure 7 shows two-dimensional (2D) and three-dimensional (3D) AFM images of single-layer and multi-layer Nb_2O_5 thin films on Si substrates annealed at different temperatures, in the $3\ \mu\text{m} \times 3\ \mu\text{m}$ scan area. The surfaces of the films are homogeneous and consist of many sphere-like grains as the film thickness increases. The root mean square (RMS) values of the surface roughness are 7.19, 7.38 and 10.92 nm for the 1, 2 and 3-layered films annealed at 200 °C, respectively and these values increased by about 3% as the annealing temperature increased from 200 to 350 °C. That is, the film roughness

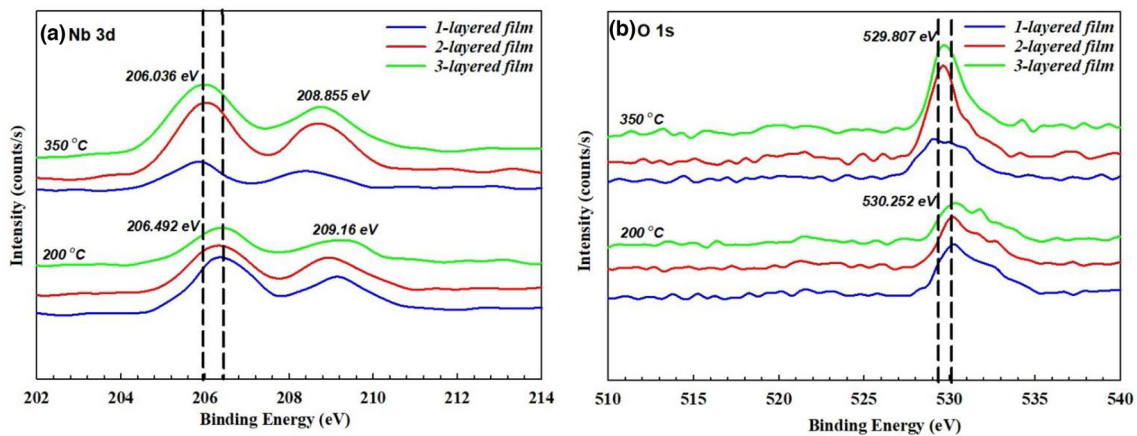


Fig. 6 XPS spectra of the Nb_2O_5 thin films annealed at 200 and 350 °C, (a) Nb 3d and (b) O 1s

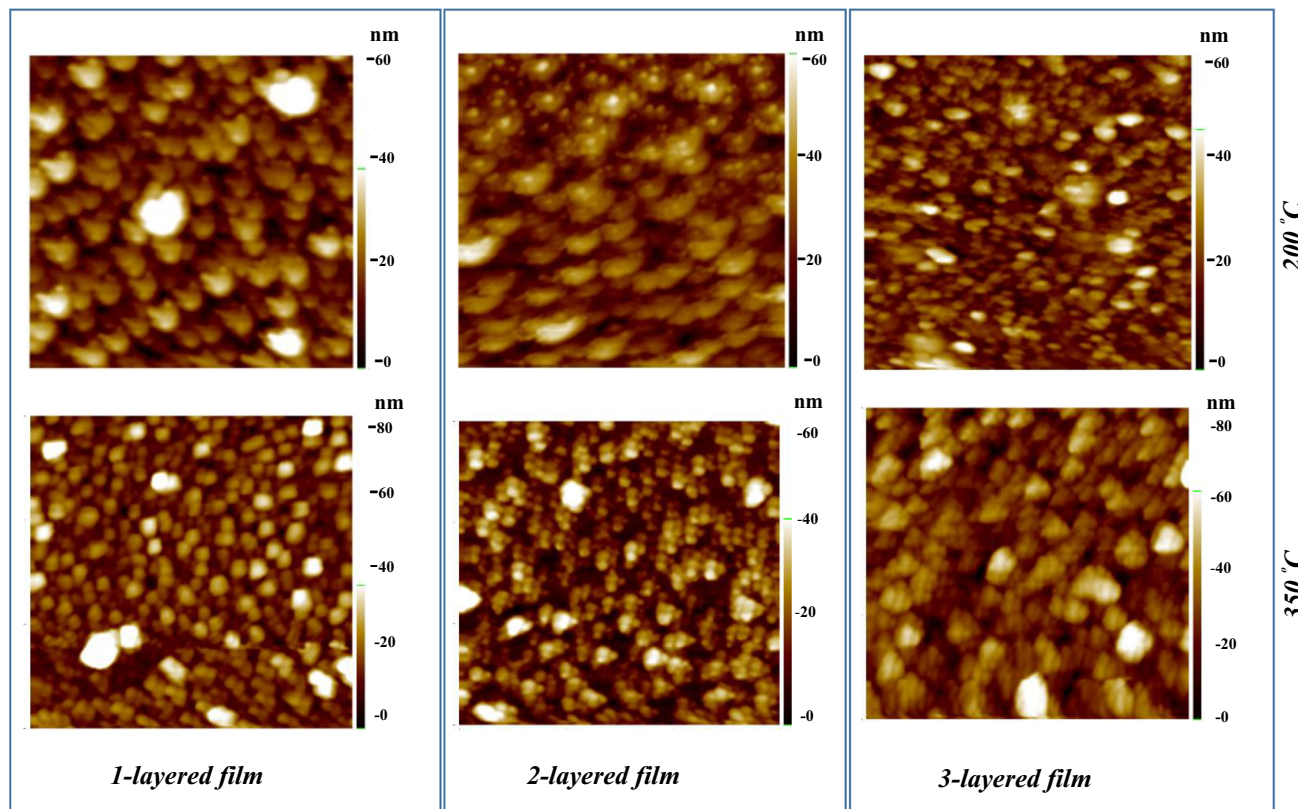


Fig. 7 2D and 3D AFM images of the single-layer and multi-layer Nb_2O_5 thin films ($3 \times 3 \mu\text{m}$) annealed at 200 and 350 °C

increased with increasing film thickness and annealing temperature, it is probably connected with the agglomeration of the grains. It corresponds to an increase in the surface area of the film, which may be a useful property for gas diffusion and transport, and it contributes significantly to the enhancement of H_2 gas sensing performances of the sensors based on the Nb_2O_5 thin films.

4 H_2 gas sensing performance of the sensors based on the Nb_2O_5 thin films

The hydrogen gas detection ability of the sensors based on the Nb_2O_5 thin films can be explained by consideration of the surface mechanism of Nb_2O_5 in the air and hydrogen atmosphere. When the oxygen is adsorbed on the Nb_2O_5 surface in the air atmosphere, charge transfer occurs between the Nb_2O_5 and the oxygen molecule. As a result of this charge transfer, the oxygen molecule decomposes into

negatively charged oxygen species [O^{2-} , O^- , and O_2^-] by capturing the electrons in the conduction band of Nb_2O_5 . That is the transfer of electrons provides the formation of a depletion layer in the near-surface region and this layer increases the working function of the grains, which means the formation of Schottky barriers at the grain boundaries. Thus, a decrease in the amount of electron concentration in the air causes an increase in the resistance of n-type Nb_2O_5 while decreasing the resistance of p-type Nb_2O_5 . When the Nb_2O_5 surface is exposed to H_2 gas, the H_2 gas molecules interact with the adsorbed oxygen, releasing the captured electrons back to the conduction band of the Nb_2O_5 . Thus, it increases the density of the charge carriers, causing a decrease in the resistance of n-type Nb_2O_5 while increasing the resistance of p-type Nb_2O_5 . A schematic of the relevant processes for n-type Nb_2O_5 is shown in Fig. 8.

It is clear that the performance of the sensors based on the Nb_2O_5 thin films will be affected by the structural and morphological properties of the film. That is, by changing various deposition/coating

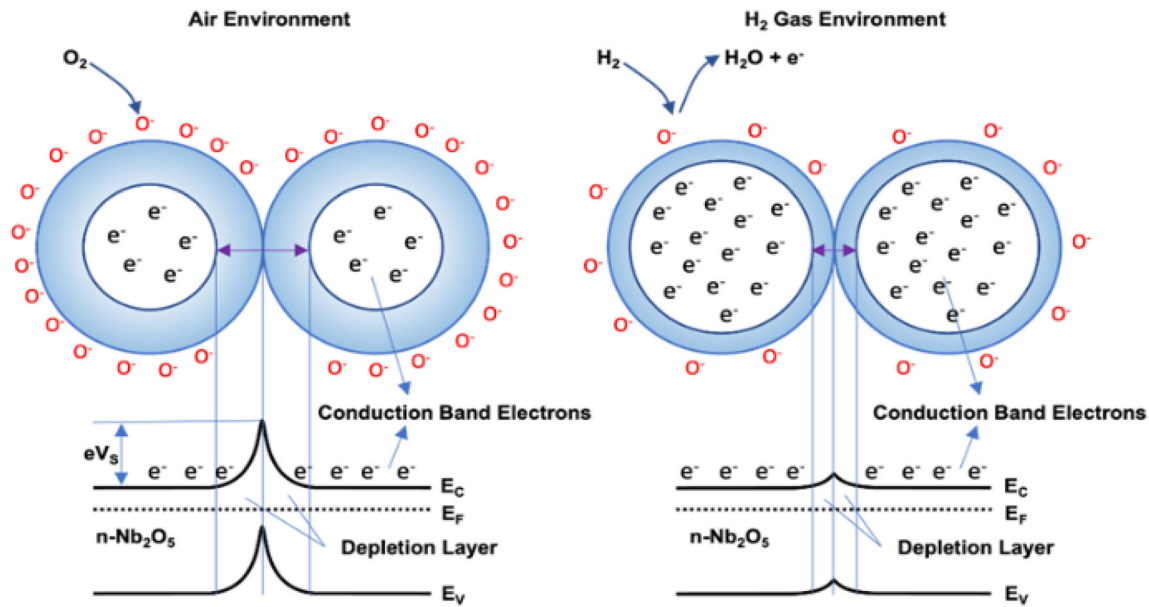


Fig. 8 Schematic illustration of the n-type Nb_2O_5 gas-sensing mechanism

parameters, a film with better properties can be obtained and thus a more sensitive sensor can be achieved. For example, changing the film thickness is a parameter, and the role of the film thickness of some metal oxides in gas detection properties has been investigated by various groups [32–36]. Korotcenkov and Cho [32] reported that they observed ambiguity in results when thin film thickness was < 50 nm, and gas sensing characteristics for films with thickness > 350 nm were significantly worse than those of films of smaller thickness. Chang et al. [33] investigated the sensing properties of the sensors based on the ZnO: Al films for CO gas by changing the film thickness from 65 to 390 nm and they observed that the thinnest film was the most sensitive. Therefore, it can be said that Nb_2O_5 films with thicknesses in the range of 60–180 nm are expected to have sensitivity as a result of interaction with the target gas. In this work, five physical parameters including gas sensitivity (response value), response time (t_{res}), recovery time (t_{rec}), stability and selectivity were defined to investigate the performances of the obtained sensors. Firstly, the sensitivity of the sensors based on the single-layer and multi-layer Nb_2O_5 thin films prepared at 200°C , named Sensor1-200, Sensor2-200 and Sensor3-200, respectively, against hydrogen (H_2) gas were defined as a function of different H_2 concentrations ranging from 90 to 1200 ppm at an operating temperature of 25°C . Based on the shift of resistance, the response of n-type Nb_2O_5

film when exposed to H_2 gas is defined as R_a/R_g , or $(R_a - R_g)/R_g$, where R_a and R_g are the measured resistances of the sensor exposed to air and target gas, respectively [37]. The obtained sensors exhibited sensing to H_2 gas, including low concentration, as seen in Fig. 9a, and the sensitivity increases linearly as $y = 0.11x$ with the increase in gas concentration, as seen in Fig. 9b. In addition, the sensitivity of the Sensor2-200 is better than other sensors. For example, as seen in Fig. 9a, the sensitivity of Sensor2-200 at 90, 180, 370, 560, 750 and 1200 ppm hydrogen gas concentrations was around 42%, 59%, 65%, 78%, 87% and 117%, respectively. The reason for its high sensitivity is thought to be related to the critical thickness and surface area of the films. Similar to our results, it has been also indicated in some reports that the sensor response will reach a maximum or minimum at a certain thickness [32, 38]. The thickness effect on the sensor performance may be explained as follows: In the deposition process of the film, i.e. when the sol-gel spin coating cycle increases, unsaturated bonds may occur due to the point defects caused by the inability of the relevant atom to introduce into the lattice. The resulting defects cause localized states in the band gap of the film. As the width of the localized states increases depending on the thickness, in other words, the defect levels increase, the sensitivity of sensors produced from thick films will decrease since these levels will act as a trap center for the electrons produced when gas is exposed to the sensor. It has

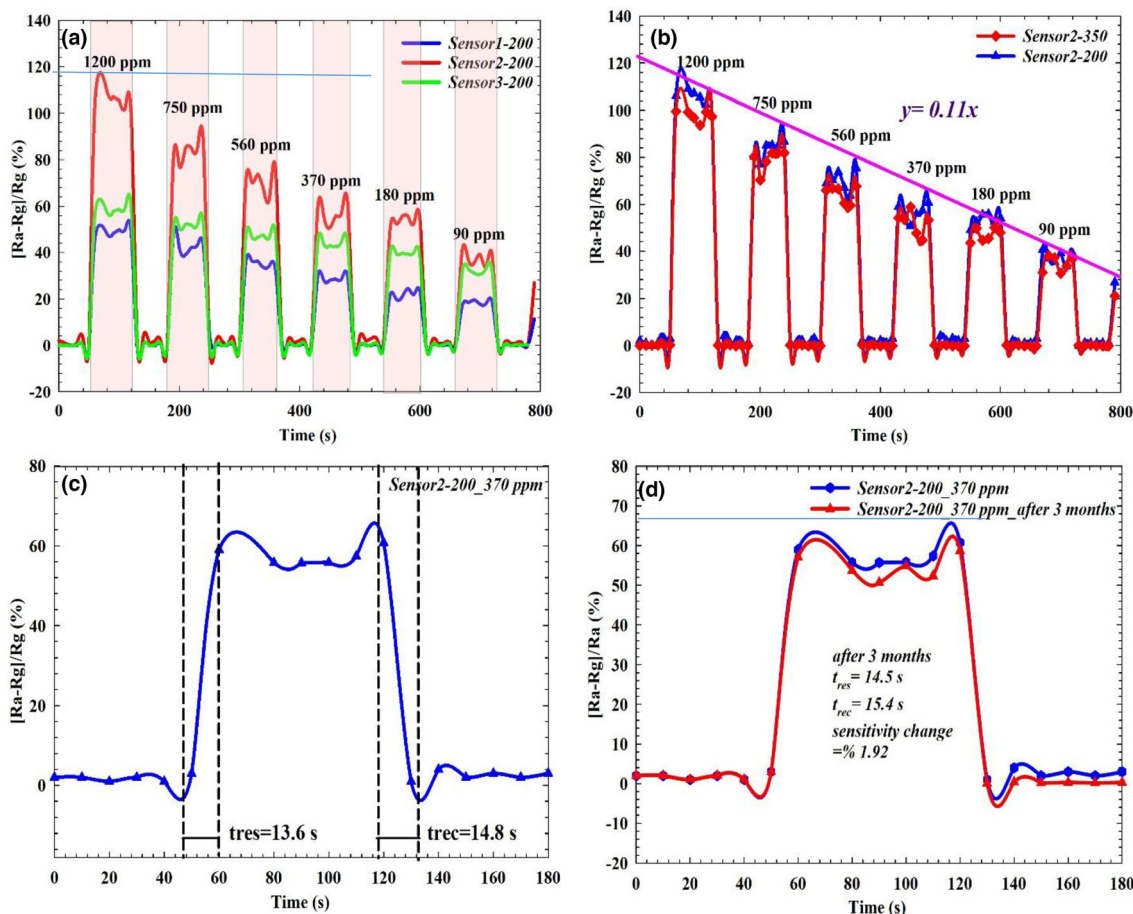


Fig. 9 Some sensor parameters when detecting H₂; (a) sensitivity at 90–1200 ppm, (b) linear sensing performance, (c) best t_{res} and t_{rec} and (d) stability over 90 days

been reported in the literature that the absorption edge is observed to be red-shifted when the thickness of the films increases [39].

Response time (t_{res}) and recovery time (t_{rec}) are important parameters for the gas sensors and t_{res} is shorter than t_{rec} for the H₂ sensor structures because the adsorption kinetics are faster than desorption kinetics, which leads to a quicker response rate [40]. For instance, for Sensor2-200, response times were 13.9, 15.4, 13.3, 13.4, 13.8 and 15.2 s, while recovery times were 15.4, 16.1, 14.8, 15.4, 15.8 and 17.1 s, at 90, 180, 370, 560, 750 and 1200 ppm hydrogen gas concentrations, respectively. Since the sensitivities of Sensor1-200, Sensor2-200 and Sensor3-200 to 50 ppm H₂ gas are around 4%, 5% and 7%, respectively, and the resistance change is observed as noise for values below this concentration, 50 ppm of H₂ can be considered as the initial gas concentration for the sensitivity of the sensors. Parameters of the Sensor2-350 whose active area consists of a 2-layered Nb₂O₅ thin

film and prepared at 350 °C are also very close to these values as seen in Fig. 9b. This is an expected result because it was seen from the FTIR results that the dehydration process of the film was almost completed at 200 °C. On the other hand, according to the AFM results, the surface properties of the annealed films at both temperatures are very close to each other. The lowest t_{res} and t_{rec} values were obtained when kept at a hydrogen gas concentration of 370 ppm and which is shown in Fig. 9c. In addition, the response and recovery times of the obtained sensor based on the Nb₂O₅ thin films have better values than that of the other type Nb₂O₅ gas sensors reported by various groups, as seen in Table 2.

The fact that the obtained sensor performance in our study is better than its counterparts in the literature can be explained as follows: In addition to the defect structure and morphology of the detector film, the electrode material, electrode geometry and the

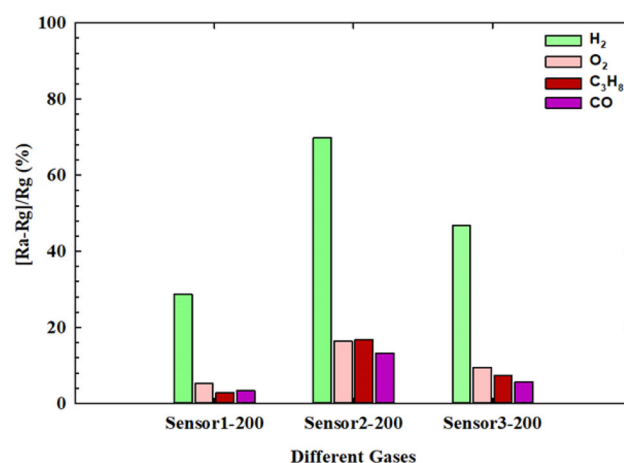
Table 2 t_{res} and t_{rec} comparison of the hydrogen sensors based on the Nb_2O_5

No	Active Material	Method	Concentration		Operating Temp. (°)	Best Sensing Performance		References
			(ppm)	(vol%)		t_{res} (s)	t_{rec} (s)	
1	Nb_2O_5 films	Anodic oxidation	10-8000	–	28–100	420	–	[16]
2	Nanoporous Nb_2O_5 films	Anodization	–	0.06–1	22–100	90	491	[17]
3	Pristine Nb_2O_5	Hydrothermal	–	0.05–2	25	83.36	310.34	[41]
4	Nb_2O_5 nanowires	Thermal oxidation	100–2000	–	25	100.2	529.8	[42]
5	Pristine Nb_2O_5	Thermal oxidation	100-10000	–	300	23	32	[43]
6	Nb_2O_5 nanorods	Hydrothermal	1000–6000	–	25	28	510	[44]
7	Nb_2O_5 nanorods	Hydrothermal	600-10000	–	25	100	125	[45]
8	Nb_2O_5 thin films	Sol-gel spin-coated	90-1200	–	25	13.3	14.8	Present work

metallization process have important effects on the detection mechanisms of the metal oxide gas sensors [46]. For example, choosing Ag electrodes with higher conductivity than platinum (Pt) or palladium (Pd) electrodes is a factor. From the geometry point of view, although the wide-spaced electrode geometry provides an increase in the active area, this leads to an increase in the transport distance of the electrons, which leads to a decrease in sensing due to the loss of charge carriers. Therefore, in our study, it is evaluated that the electrodes having interdigital geometry formed by determining the distance between the fingers of 65 μm finger width as 500 μm minimizes the loss of charge carrier during the gas detection process. In addition, the contact series resistance can be reduced by preventing the formation of the Schottky barrier in the Ag electrode/ Nb_2O_5 sensing layer, thanks to the optimization of metallization at 7 μm thickness with the aerosol printing and sintering temperature process. Besides, an important approach is using the circular substrates for the first time in these structures, which is our own idea; because on the surface of the circular substrates, the Nb_2O_5 solution is homogeneously dispersed by the effect of centrifugal force, thus avoiding the corner effects.

As a final step, the stability and reliability-selectivity of the gas sensors should also be evaluated. Among them, considering the stability, which is the ability of the sensor to keep its properties constant when operated for a long time, it was seen that good results were obtained for the produced sensors. For example, Fig. 9d shows the resistance change after 3 months for Sensor2-200, which has the best sensor performance when kept at a hydrogen gas

concentration of 370 ppm. It is a rather significant result that the loss of sensitivity remained almost unchanged at $\sim 1.92\%$ after 3 months. In addition, reliability-selectivity is described as the ability of the sensor to selectively detect a single analyte gas or a group of analyte gases. In order to determine the reliability-selectivity behavior of sensors based on Nb_2O_5 , by looking at the sensitivity of the produced sensors to H_2 (hydrogen), CO (carbon monoxide), O_2 (oxygen) and C_3H_8 (propane) gases at RT were compared. In this measurement, the concentration of each gas was around 400 ppm. It was seen that the responsiveness to CO , C_3H_8 and O_2 gases was very low, as seen in Fig. 10. That is, in the presence of oxygen, for example, air, the cross-sensitivity of the sensor to oxygen is important in many applications. In order to understand whether the presence of more than normal oxygen content in the environment suppresses the hydrogen sensitivity of the sensor, different amounts

**Fig. 10** Selectivity pattern of the Ag/ Nb_2O_5 thin film sensors at RT

of pure oxygen were included in the test environment and the sensitivity of the sensor to oxygen was examined. The results show that the developed sensors have a very low sensitivity to oxygen [47, 48]. Besides, it is necessary to determine the cross-sensitivity of a hydrogen sensor to oxygen in environments with oxygen such as air, or in a vacuum chamber with very low oxygen content. This result is a remarkable indication that the produced sensors have high selectivity towards H₂ gas. It should be noted that the resistance change, i.e. sensitivity, of the sensors to CO, C₃H₈ and O₂ gases below 400 ppm was at the noise level. For example, Sensor1-200 and Sensor3-200's sensitivity to CO, and C₃H₈ and O₂ gases at 350 ppm were at the 1% levels, and Sensor2-200 at 2%, and quite noisy. In light of this evaluation, the initial value of the sensitivity of the sensors for these gases can be accepted as 400 ppm.

5 Conclusion

In summary, Nb₂O₅ thin films with different thicknesses have been successfully coated on the Si substrates with an easy, simple and cost-effective sol-gel spin coating system and annealed at low temperatures. Interdigital Ag electrodes were printed on the surface of the films to form gas sensors. Afterward, the gas-sensing properties of the produced sensors were comprehensively studied by means of 5 parameters; sensitivity, response time, recovery time, stability and selectivity. Despite being operated at room temperature, the sensors demonstrated high sensitivity and short response/recovery times, better than the best known. In addition, the film thickness range of > 60 nm and < 180 nm was evaluated to be the critical thickness for the performance of Ag/Nb₂O₅ thin film sensors. Specifically, the sensor based on a 2-layered film (108 nm thick) showed a highly linear sensing performance with the increase in gas concentration. The sensitivity of the Sensor2-200 at 90, 180, 370, 560, 750 and 1200 ppm hydrogen gas concentrations was around 42%, 59%, 65%, 78%, 87% and 117%, respectively. Thus, especially sensors with an active area of 108 nm Nb₂O₅ thin films are more suitable for detecting H₂ gas with concentrations as low as a few ppm and are able to use in hydrogen-based energy systems.

Acknowledgements

This work was supported by the Presidency of Strategy and Budget (Turkey) under Project number 2019K12-149045 and G.U. BAP under Project number of 70/2020-01.

Author contributions

HAK implemented the research scheme and wrote the manuscript. All authors contributed to the study conception and design. All authors read and approved the final manuscript.

Funding

The authors have not disclosed any funding.

Data availability

The data used to support the findings of this study are included in the article.

Declarations

Conflict of interest The authors declare that they have no known competing financial interests or personal relationships that could have appeared to influence the work reported in this paper.

Ethical approval This article does not contain any studies involving humans and animals performed by any of the authors.

References

1. H. Sun, H. Lv, J. Alloy. Comp. **823**: 153742(2020)
2. N. Usha, R. Sivakumar, C. Sanjeeviraja, Y. Kuroki, J. Alloy Compd. **649**, 112–121 (2015)
3. S.S. More, P.A. Patil, K.D. Kadam, H.S. Patil, S.L. Patil, A.V. Pawar, T.D. Dongale, Results Phys. **12**, 1946–1955 (2019)
4. J.M.F. Lucas, S. Soreto Teixeira, S.R. Gavinho, P.R. Prezas, C.C. Silva, A.J.M. Sales, M.A. Valente, A.F. Almeida, F.N. Freire, C.C.M. Salgueiro, J.F. Nunes, M.P.F. Graça, J. Mater. Sci.: Mater. Electron. **30**, 11346–11353 (2019)

5. N. Hossain, O. Günes, C. Zhang, C. Koughia, Y. Li, S.-J. Wen, R. Wong, S. Kasap, Q. Yang, *J. Mater. Sci.: Mater. Electron.* **30**, 9822–9835 (2019)
6. R.A. Rani, A.S. Zoofakar, A.P. O’Mullane, M.W. Austin, K. Kalantar-Zadeh, *J. Mater. Chem. A* **2**(38), 15683–15703 (2014)
7. M. Mazur, M. Szymańska, D. Kaczmarek, M. Kalisz, D. Wojcieszak, J. Domaradzki, F. Placido, *Appl. Surf. Sci.* **301**, 63–69 (2014)
8. S. Li, H. Shen, J. Chen, Y. Jiang, L. Sun, A. Raza, Y. Xu, *J. Mater. Sci.: Mater. Electron.* **30**, 19871–19879 (2019)
9. Rps Patil, Ar. Patil, Sh. Mujavar, Sb. Sadale, *J. Mater. Sci.: Mater. Electron.* **16**, 35–41 (2005)
10. S. Ouendi, C. Arico, F. Blanchard, J.L. Codron, X. Wallart, P.L. Taberna, P. Roussel, L. Clavier, P. Simon, C. Lethien, *Energy Stor. Mater.* **16**, 581–588 (2019)
11. K.N. Chen, C.M. Hsu, J. Liu, Y.C. Liou, C.F. Yang, *Micromachines* **7**(9), 151 (2016)
12. M. Danish, A. Pandey, *J. Mater. Sci.: Mater. Electron.* **27**, 6939–6946 (2016)
13. V. Khorramshahi, J. Kaamdel, R. Yousefi, *J. Mater. Sci.: Mater. Electron.* **29**, 14679–14688 (2018)
14. M.I. Khan, K.A. Bhatti, R. Qindeel, H.S. Althobaiti, N. Alonizan, *Results Phys.* **7**, 1437–1439 (2017)
15. M.I. Khan, K.A. Bhatti, R. Qindeel, N. Alonizan, H.S. Althobaiti, *Results Phys.* **7**, 651–655 (2017)
16. T. Hyodo, J. Ohoka, Y. Shimizu, M. Egashira, *Sens. Actuators B Chem.* **117**(2), 359–366 (2006)
17. R.A. Rani, A.S. Zoofakar, J.Z. Ou, M.R. Field, M. Austin, K. Kalantar-zadeh, *Sens. Actuators B Chem.* **176**, 149–156 (2013)
18. D.C. Castro, R.P. Cavalcante, J. Jorge, M.A. Martines, L. Oliveira, G.A. Casagrande, Jr.A. Machulek, *J. Braz Chem. Soc.* **27**, 303–313 (2016)
19. P. Griesmar, G. Papin, C. Sanchez, *J. Livage, Chem. Mater.* **3**(2), 335–339 (1991)
20. C.D. Gomez, J.E. Rodríguez-Paez, *Process. Appl. Ceram.* **12**(3), 218–229 (2018)
21. N.S. Rao, S. Dhamodaran, A.P. Pathak, P.K. Kulriya, Y.K. Mishra, F. Sing, D. Kabiraj, J.C. Pivin, D.K. Avasthi, *Methods Phys. Res. Sect. B: Beam Interact. Mater. At.* **264**(2), 249–253 (2007)
22. B. Orel, M. Maček, J. Grdadolnik, A. Meden, *J. Solid State Electrochem.* **2**(4), 221–236 (1998)
23. V.S. Braga, F.D.C. Garcia, J.A. Dias, S.C. Dias, *J. Therm. Anal. Calorim.* **92**(3), 851–855 (2008)
24. P. Amaravathy, S. Sowndarya, S. Sathyanarayanan, N. Rajendran, *Surf. Coat. Technol.* **244**, 131–141 (2014)
25. K.M. Eblagon, A. Malaika, K. Ptaszynska, M.F.R. Pereira, J.L. Figueiredo, *Nanomaterials* **10**, 1685 (2020)
26. Y.Q. Zhang, Z. Li, T. Ling, S.A. Kulinich, *J. Mater. Chem. A* **4**(22), 8700–8706 (2016)
27. X. Ma, Y. Chen, H. Li, X. Cui, Y. Lin, *Mater. Res. Bull.* **66**, 51–58 (2015)
28. J.M. Jehng, I.E. Wachs, *Chem. Mater.* **3**(1), 100–107 (1991)
29. F. Lenzmann, V. Shklover, K. Brooks, M. Grätzel, *J. Sol–Gel Sci. Technol.* **19**(1), 175–180 (2000)
30. B. Liu, H. Wang, Y. Chen, J. Wang, L. Peng, L. Li, *J. Alloys Compd.* **682**, 584–589 (2016)
31. K.W. Chen, L.S. Chen, C.M. Chen, *J. Mater. Sci.: Mater. Electron.* **30**(16), 15105–15115 (2019)
32. G. Korotcenkov, B.K. Cho, *Sens. Actuators B Chem.* **142**(1), 321–330 (2009)
33. J.F. Chang, H.H. Kuo, I.C. Leu, M.H. Hon, *Sens. Actuators B Chem.* **84**, 258–264 (2002)
34. R. Godbole, V.P. Godbole, P.S. Alegaonkar, S. Bhagwat, *New. J. Chem.* **41**, 11807–11816 (2017)
35. V.V. Ganbavle, S.V. Mohite, G.L. Agawane, J.H. Kim, K.Y. Rajpure, *J. Colloid Interface Sci.* **451**, 245–254 (2015)
36. G. Korotcenkov, V. Brinzari, A. Cernevschi, M. Ivanov, V. Golovanov, A. Cornet, J. Morante, *Thin Solid Films* **460**, 315–323 (2004)
37. F. Xu, H.P. Ho, *Micromachines* **8**(11), 333 (2017)
38. W.Y. Chung, G. Sakai, K. Shimano, N. Miura, D.D. Lee, N. Yamazoe, *Sens. Actuators B Chem.* **46**(2), 139–145 (1998)
39. M.B. Rabeih, N. Khedmi, M.A. Fodha, M. Kanzari, *Energy Procedia* **44**, 52–60 (2014)
40. D. Pukazhselvan, N. Nasani, T. Yang, D. Ramasamy, A. Shaula, D.P. Fagg, *Appl. Surf. Sci.* **472**, 99–104 (2019)
41. A. Mirzaei, G.J. Sun, J.K. Lee, C. Lee, S. Choi, H.W. Kim, *Ceram. Int.* **43**(6), 5247–5254 (2017)
42. Z. Wang, Y. Hu, W. Wang, X. Zhang, B. Wang, H. Tian, H. Gu, *Int. J. Hydrog. Energy* **37**(5), 4526–4532 (2012)
43. S. Park, S. Park, S. Lee, H.W. Kim, C. Lee, *Sens. Actuators B: Chem.* **202**, 840–845 (2014)
44. Y. Zou, J. He, Y. Hu, R. Huang, Z. Wang, Q. Gu, *RSC Adv.* **8**(30), 16897–16901 (2018)
45. J. Yu, K.W. Cheung, W.H. Yan, D. Ho, *IEEE Electron. Device Lett.* **37**(9), 1223–1226 (2016)
46. S. Saukko, V. Lantto, *Thin solid films* **436**(1), 137–140 (2003)
47. G. Korotcenkov, *Handbook of gas sensor materials* (Springer, New York, 2013), pp.197–220
48. T. Galonska, C. Senft, W. Widanarto, O. Senftleben, I. Eisele, H.P. Frerichs, Ch. Wilbertz, *Sensors* **1**, 1036–1039 (2007)

Publisher’s Note Springer Nature remains neutral with regard to jurisdictional claims in published maps and institutional affiliations.

Springer Nature or its licensor (e.g. a society or other partner) holds exclusive rights to this article under a publishing agreement with the author(s) or other

rightsholder(s); author self-archiving of the accepted manuscript version of this article is solely governed by the terms of such publishing agreement and applicable law.